Available online at www.sciencedirect.com
ScienceDirect
Mathematics and Computers in Simulation xxx (xxxx) xxx
MATHEMATICS AND COMPUTERS IN SIMULATION
www.elsevier.com/locate/matcom

Original articles

Pulsatile flow and heat transfer of blood in an overlapping vibrating atherosclerotic artery: A numerical study

G.C. Shit[a,*], S. Maiti[a], M. Roy[b], J.C. Misra[c]

[a] Department of Mathematics, Jadavpur University, Kolkata 700032, India
[b] Department of Mathematics, Sammilani Mahavidyalaya, Kolkata 700094, India
[c] Centre for Theoretical Studies, Indian Institute of Technology, Kharagpur 721302, India

Received 24 September 2018; received in revised form 22 March 2019; accepted 26 June 2019
Available online xxxx

Highlights

- Numerically studied MHD pulsatile flow of blood and heat transfer in the stenosed artery.
- Body acceleration due to vibration is considered for simulating blood flow.
- Microrotation of microparticles taken into account suspended in the porous vascular tube.
- WSS increases significantly for a rise in the permeability of the porous medium.
- Fluid acceleration enhances with an increase in amplitude of body acceleration.

Abstract

The paper is devoted to a numerical investigation of the pulsatile flow of blood through a porous overlapping constricted artery under the influence of an externally imposed magnetic field and vibration environment that is originated from the body force. Blood is considered as micropolar fluid. The heat transfer phenomenon arising out of viscous dissipation is also studied. The problem is solved numerically by developing a Crank–Nicolson finite difference scheme after transforming the original governing equations from the physical domain to a rectangular computational domain. The computational results for the velocity and temperature distributions, fluid acceleration, skin friction and Nusselt number are presented graphically for different values of the physical parameters. The study shows that the Nusselt number increases with rise in Prandtl number and Brinkman number both and that owing to the dissipation of energy caused by blood viscoelasticity and magnetic field effect, during pulsatile flow of blood, the heat transfer rate at the wall of the artery is enhanced.

Keywords: Micropolar fluid; Overlapping stenosis; Porous medium; Body acceleration

1. Introduction

Usually when blood flows through large arteries at a high shear rate, it can be treated as a homogeneous fluid and its flow behaviour can be described by a Newtonian model (MacDonald [20], Caro et al. [4]). Of course, Liepsch [19] carried out an experimental study to show that blood can behave like a non-Newtonian fluid, when

* Corresponding author.
E-mail address: gopal_iitkgp@yahoo.co.in (G.C. Shit).

https://doi.org/10.1016/j.matcom.2019.06.015
0378-4754/

the shear rate is low, even in large arteries. In the case of most small arteries, the shear rate is as low as 0.1 s^{-1}, it is recommended that blood should be described by a non-Newtonian model. Chien [8] pointed out that in some pathological conditions (e.g. several myocardial infarction, hypertension and several other cardiovascular disorders), the non-Newtonian behaviour of blood is highly prominent. In various hemodynamical studies, depending on the objective of the study, different authors [47,49] have used different non-Newtonian models for blood flow. The concept of micropolar fluid model initiated by Eringen [10,11] has been used in several studies of blood flow dynamics. This model is particularly suitable, when it is intended to account for the rotation of the microparticles (e.g. erythrocytes, leucocytes, thrombocytes, etc.) suspended in blood. Some boundary conditions for the study of the dynamical behaviour of a micropolar fluid were proposed by Kirwan [16]. Muthu et al. [34] examined the influence of wall properties on the peristaltic motion of a micropolar fluid. Several authors [2,6,13,42,50] considered blood as a micropolar fluid in various studies conducted by them. Among them, Shit and Roy [42] examined the effect of slip velocity on peristaltic transport of a magneto-micropolar fluid through a non-uniform porous channel. Hogan and Henricksen [13] discussed the use of micropolar fluid model in their study of blood flow in an artery in the presence of an idealized stenosis. These studies were made by considering the presence of an external magnetic field/ body acceleration.

Flow of a micropolar fluid on a microchannel under the action of an AC field was discussed by Misra et al. [24]. On basis of the theoretical study, the authors have reported estimates of blood flow in bio-fluidic devices. Chandra and Misra [5] studied the influence of Hall current on the boundary layer flow of an electrically conducting fluid and also discussed the application of the model to the dynamics of blood flow.

Studies on blood flow through porous vessels are receiving growing attention of researchers, owing to the observation that appreciable changes occur in blood flow behaviour occur due to the porosity of blood vessels. Khalid and Vafai [15] studied the role of porosity on blood flow and its impact on temperature distribution in living biological tissues during hyperthermic treatment. A numerical study of blood flow in arteries was performed by He et al. [12] with an aim to understand the role of porosity in microvascular dysfunction. Tanveer et al. [48] have considered the modified Darcy's law in Sisko fluid model to study the porosity effect in ureteral peristalsis and arterial blood flow.

It is known that of arterial diseases like atherosclerosis (also referred to sclerosis) brings about various types of flow disorders in arteries. Some of the initial studies on this problem were carried out by Lee and Fung [17] and Young [51]. Subsequently different aspects of blood flow in stenosed arteries under various conditions have been carried out by several authors (Srivastava [45], Misra and his coworkers [22,23,27,29,31–33,43,44]).

However, all the aforementioned studies have been restricted to cases, where blood flow takes place in the presence of a single or multiple stenoses. Raihi et al. [36] made an attempt to study blood flow in the presence of overlapping stenosis, by using both analytical and computational methods. The study was further extended by Elcot and Abbas [9], who considered blood flow through a catheterized artery in the presence of overlapping stenosis.

Recently, some other studies on hemodynamical modelling have been reported by several researchers [1,3,14,39,40] by treating blood as an electrically conducting fluid. In [40], the authors have considered blood flow in a diseased artery, where an abdominal aortic aneurysm has been developed. In [39], by using computational methods, the same authors have studied heat transfer during blood flow in an arterial segment of slowly varying cross-section. Misra and Pal [26] developed a mathematical model for the study of the effect of externally imposed body acceleration on blood flow in arteries. A comprehensive study was conducted by Misra et al. [30] for electro-osmotic flow of a viscoelastic fluid with special reference to arterial blood flow. The study provides novel insight for the design of bio-sensing and micro-fluidic devices. Misra and Maiti [25] put forward a theoretical study for the peristaltic transport of a rheological fluid. The analysis bears the promise of exploring the movement of various physiological fluids, by way of parametric variation. In these studies, the authors have tried to determine the ranges of magnetic field intensity, where clinical disorder does not take place.

Although characteristics of blood flow depend mostly on the pumping action of the heart, as discussed in a recent paper by Misra et al. [21], the behaviour of blood flow can be greatly affected, when the human body is subject to a vibration environment. When a man works with a jack hammer or a grill machine or when he drives a car, partial/whole body vibration takes place in the human body and this results in body acceleration. The effects of body acceleration on blood flow have been studied by several authors [7,28,35,38,41,46]. Shit and Roy [41] as well as Shit and Majee [38] discussed two different problems related to the effect of heat transfer on blood flow in arteries subject to body acceleration. But, the porosity of the arterial wall was not taken into account. Neither did any of them consider the presence of magnetic field.

Please cite this article as: G.C. Shit, S. Maiti, M. Roy et al., Pulsatile flow and heat transfer of blood in an overlapping vibrating atherosclerotic artery: A numerical study, Mathematics and Computers in Simulation (2019), https://doi.org/10.1016/j.matcom.2019.06.015.

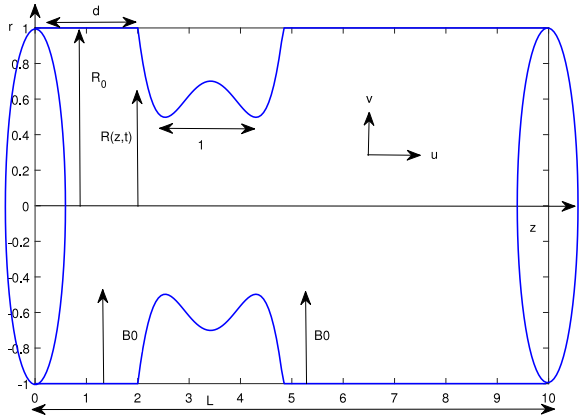

Fig. 1. Schematic diagram of the model.

In view of this we have made an endeavour in this paper to explore the influence of heat transfer on the pulsatile flow behaviour of blood in an arterial segment subject to a vibration environment. The arterial segment is considered to have overlapping stenosis. Because of the considerations, the study will be closer to a pathological condition of the arterial system and is likely to have variable applications in clinical practice, particularly when the body is subject to an electromagnetic field, as in MRI. Because of the complexity of the problem, we had to develop a suitable computational technique to achieve our objectives.

2. Mathematical formulation

Let us consider the unsteady laminar flow of blood in a porous atherosclerotic artery (cf. Fig. 1). The flow is considered as two-dimensional and axially symmetric. With an aim to take into account the effect of microrotation of erythrocytes, thrombocytes and other microparticles, blood will be treated here as a micropolar fluid. The influence of body acceleration on pulsatile blood flow is also paid due attention. The system is considered to be under the action of a transverse magnetic field. Let (r^*, θ^*, z^*) be the co-ordinates of any material point in the blood flow domain, where z^*-axis is taken along the axis of the artery and r^* is measured along the radial direction. We denote by u^* and v^* the dimensional components of blood velocity along the axial and radial directions respectively and by w^* the microrotational velocity of micro-particles of blood. Considering axisymmetry, we assume that the flow variation is independent of θ^*. Owing to the above considerations, the governing equations of motion can be written as

$$\frac{\partial u^*}{\partial z^*} + \frac{v^*}{r^*} + \frac{\partial v^*}{\partial r^*} = 0, \tag{1}$$

$$\rho\left(\frac{\partial u^*}{\partial t^*} + u^*\frac{\partial u^*}{\partial z^*} + v^*\frac{\partial u^*}{\partial r^*}\right) = -\frac{\partial p^*}{\partial z^*} + (\mu + k)\left(\frac{\partial^2 u^*}{\partial r^{*2}} + \frac{1}{r^*}\frac{\partial u^*}{\partial r^*} + \frac{\partial^2 u^*}{\partial z^{*2}}\right) + k\left(\frac{\partial w^*}{\partial r^*} + \frac{w^*}{r^*}\right) - \sigma B_0^2 u^* + \rho G^*(t^*) - \frac{\mu}{K_p^*}u^*, \tag{2}$$

$$\rho\left(\frac{\partial v^*}{\partial t^*} + u^*\frac{\partial v^*}{\partial z^*} + v^*\frac{\partial v^*}{\partial r^*}\right) = -\frac{\partial p^*}{\partial r^*} + (\mu + k)\left(\frac{\partial^2 v^*}{\partial r^{*2}} + \frac{1}{r^*}\frac{\partial v^*}{\partial r^*} - \frac{v^*}{r^{*2}} + \frac{\partial^2 v^*}{\partial z^{*2}}\right) - k\frac{\partial w^*}{\partial z^*} - \frac{\mu}{K_p^*}v^*, \tag{3}$$

$$\rho j\left(\frac{\partial w^*}{\partial t^*} + u^*\frac{\partial w^*}{\partial z^*} + v^*\frac{\partial w^*}{\partial r^*}\right) = -k\left(2w^* + \frac{\partial u^*}{\partial r^*} - \frac{\partial v^*}{\partial z^*}\right) + \gamma\left(\frac{\partial^2 w^*}{\partial r^{*2}} + \frac{1}{r^*}\frac{\partial w^*}{\partial r^*} - \frac{w^*}{r^{*2}} + \frac{\partial^2 w^*}{\partial z^{*2}}\right), \tag{4}$$

Please cite this article as: G.C. Shit, S. Maiti, M. Roy et al., Pulsatile flow and heat transfer of blood in an overlapping vibrating atherosclerotic artery: A numerical study, Mathematics and Computers in Simulation (2019), https://doi.org/10.1016/j.matcom.2019.06.015.

and

$$\frac{\partial T^*}{\partial t^*}+u^*\frac{\partial T^*}{\partial z^*}+v^*\frac{\partial T^*}{\partial r^*}=\frac{\kappa_0}{\rho C_p}\left(\frac{\partial^2 T^*}{\partial r^{*2}}+\frac{1}{r^*}\frac{\partial T^*}{\partial r^*}+\frac{\partial^2 T^*}{\partial z^{*2}}\right)+\frac{\sigma B_0^2}{\rho C_p}u^{*2}+\frac{(\mu+k)}{\rho C_p}\left[2\left(\frac{\partial u^*}{\partial z^*}\right)^2+\left(\frac{\partial u^*}{\partial r^*}\right)^2\right], \tag{5}$$

where ρ is the blood density, p^* the blood pressure, μ the coefficient of dynamic viscosity of blood, k the rotational viscosity, σ the electrical conductivity, B_0 the applied magnetic field strength, γ the spin gradient viscosity satisfying $\gamma = j(\mu + k/2)$, j is the micro-gyration constant. T^* represents the temperature, C_p the specific heat at constant pressure. κ_0 denotes thermal conductivity and K_p stands for the permeability of porous medium. In the governing equations, we have neglected the effect of induced magnetic field due to small magnetic Reynolds number ($R_m \ll 1$), the electrical conductivity of blood being very low. For $t^* > 0$, the flow is assumed to have a periodic body acceleration $G^*(t^*)$ that appears in Eq. (2) and has an expression of the form

$$G^*(t^*) = a^*(cos\omega_b t^* + \phi_g), \tag{6}$$

where a^*, ω_b and ϕ_g denote respectively the amplitude, frequency and phase difference of body acceleration.

The geometry of the stenosis (cf. Fig. 1) can be described mathematically in non-dimensional form as

$$R(z,t)=\begin{cases} R_0\left[1-\frac{11}{32}l^3(z-d)+\frac{47}{48}l^2(z-d)^2-l(z-d)^3+\frac{1}{3}(z-d)^4\right]\times \\ \qquad (1+K_r sin(t+\phi_r)); & \text{when } d<z<d+l_0, \\ R_0[1+K_r sin(t+\phi_r)]; & \text{elsewhere} \end{cases} \tag{7}$$

in which R_0 is the radius of the artery in the normal physiological state, K_r the amplitude of arterial motion and ϕ_r the phase difference between pulsation of wall motion and pressure gradient.

Let us now introduce the following non-dimensional variables:

$$z=\frac{z^*}{R_0},\quad r=\frac{r^*}{R_0},\quad u=\frac{u^*}{\omega R_0},\quad v=\frac{v^*}{\omega R_0},\quad w=\frac{w^*}{\omega},\quad p=\frac{p^*}{\mu\omega},\quad t=\omega t^*,$$
$$J=\frac{j}{R_0^2},\quad \theta=\frac{T^*-T_\infty}{T_w-T_\infty},\quad R=\frac{R^*}{R_0},\quad K_p=\frac{K_p^*}{R_0^2},\quad a_0=\frac{\rho R_0 a_0^*}{\mu\omega},\quad J=\frac{j}{R_0^2}.$$

In terms of these dimensionless variables the Eqs. (1)–(5) become

$$\frac{\partial u}{\partial z}+\frac{v}{r}+\frac{\partial v}{\partial r}=0, \tag{8}$$

$$\alpha^2\left(\frac{\partial u}{\partial t}+u\frac{\partial u}{\partial z}+v\frac{\partial u}{\partial r}\right)=-\frac{\partial p}{\partial z}+(1+K)\left(\frac{\partial^2 u}{\partial r^2}+\frac{1}{r}\frac{\partial u}{\partial r}+\frac{\partial^2 u}{\partial z^2}\right)+K\left(\frac{\partial w}{\partial r}+\frac{w}{r}\right)-Ha^2u+G(t)-\frac{1}{K_p}u, \tag{9}$$

$$\alpha^2\left(\frac{\partial v}{\partial t}+u\frac{\partial v}{\partial z}+v\frac{\partial v}{\partial r}\right)=-\frac{\partial p}{\partial r}+(1+K)\left(\frac{\partial^2 v}{\partial r^2}+\frac{1}{r}\frac{\partial v}{\partial r}-\frac{v}{r^2}+\frac{\partial^2 v}{\partial z^2}\right)-k\frac{\partial w}{\partial z}-\frac{1}{K_P}v, \tag{10}$$

$$\alpha^2 J\left(\frac{\partial w}{\partial t}+u\frac{\partial w}{\partial z}+v\frac{\partial w}{\partial r}\right)=-K\left(2w+\frac{\partial u}{\partial r}-\frac{\partial v}{\partial z}\right)+m\left(\frac{\partial^2 w}{\partial r^2}+\frac{1}{r}\frac{\partial w}{\partial r}-\frac{w}{r^2}+\frac{\partial^2 w}{\partial z^2}\right), \tag{11}$$

$$\alpha^2 P_r\left(\frac{\partial \theta}{\partial t}+u\frac{\partial \theta}{\partial z}+v\frac{\partial \theta}{\partial r}\right)=\left(\frac{\partial^2\theta}{\partial r^2}+\frac{1}{r}\frac{\partial\theta}{\partial r}+\frac{\partial^2\theta}{\partial z^2}\right)+BrHa^2u^2+(1+K)Br\left[2\left(\frac{\partial u}{\partial z}\right)^2+\left(\frac{\partial u}{\partial r}\right)^2\right], \tag{12}$$

Please cite this article as: G.C. Shit, S. Maiti, M. Roy et al., Pulsatile flow and heat transfer of blood in an overlapping vibrating atherosclerotic artery: A numerical study, Mathematics and Computers in Simulation (2019), https://doi.org/10.1016/j.matcom.2019.06.015.

where the non-dimensional parameters appearing in Eqs. (9)–(12) are defined as the ratio of viscosity coefficients $K = \frac{k}{\mu}$, the material constant $m = \frac{\gamma}{\mu R_0^2}$ is called the micropolar parameter. Womersley number $\alpha = R_0\sqrt{\frac{\rho\omega}{\mu}}$, Hartmann number $Ha = R_0 B_0\sqrt{\frac{\sigma}{\mu}}$, Prandtl number $P_r = \frac{\mu C_p}{\kappa_0}$, Brinkman number $Br = E_c P_r$ and Eckert number $E_c = \frac{\omega^2 R_0^2}{C_p(T_w - T_\infty)}$.

In terms of the non-dimensional quantities $a_0 = \frac{\rho R_0 a^*}{\mu\omega}$, $b = \frac{\omega_b}{\omega}$, the expression for the body acceleration (6) has the form

$$G(t) = a_0 \cos(bt + \phi_g) \quad with \quad t \geq 0. \tag{13}$$

Also the non-dimensional form of axial pressure gradient is assumed to be

$$-\frac{\partial P(t)}{\partial z} = \bar{K} + A_p \cos(t), \tag{14}$$

where $\bar{K}$ and A_p stand respectively for the mean amplitude of pressure gradient and amplitude of the pulsatile component that give rise to systolic and diastolic pressures. It is clear from Eqs. (9)–(12) that when K and m are set equal to zero, the system of equations reduces to that for a classical Newtonian fluid model.

We shall now use long wavelength approximation ($\frac{R}{\lambda} \ll 1$), considering the radius R of the arterial lumen to be sufficiently smaller than the wavelength λ of pressure wave, so that the axial viscous transport terms are negligible. In this case, Eq. (10) reduces to $\frac{\partial p}{\partial r} = 0$, while the other equations become

$$\frac{\partial u}{\partial z} + \frac{v}{r} + \frac{\partial v}{\partial r} = 0, \tag{15}$$

$$\alpha^2\left(\frac{\partial u}{\partial t} + u\frac{\partial u}{\partial z} + v\frac{\partial u}{\partial r}\right) = -\frac{\partial p}{\partial z} + (1+K)\left(\frac{\partial^2 u}{\partial r^2} + \frac{1}{r}\frac{\partial u}{\partial r}\right) + K\left(\frac{\partial w}{\partial r} + \frac{w}{r}\right) - Ha^2 u + G(t) - \frac{1}{K_p}u, \tag{16}$$

$$\alpha^2 J\left(\frac{\partial w}{\partial t} + u\frac{\partial w}{\partial z} + v\frac{\partial w}{\partial r}\right) = -K\left(2w + \frac{\partial u}{\partial r} - \frac{\partial v}{\partial z}\right) + m\left(\frac{\partial^2 w}{\partial r^2} + \frac{1}{r}\frac{\partial w}{\partial r} - \frac{w}{r^2}\right), \tag{17}$$

$$\alpha^2 P_r\left(\frac{\partial \theta}{\partial t} + u\frac{\partial \theta}{\partial z} + v\frac{\partial \theta}{\partial r}\right) = \left(\frac{\partial^2 \theta}{\partial r^2} + \frac{1}{r}\frac{\partial \theta}{\partial r}\right) + Br\,Ha^2 u^2 + (1+K)Br\left[2\left(\frac{\partial u}{\partial z}\right)^2 + \left(\frac{\partial u}{\partial r}\right)^2\right]. \tag{18}$$

The boundary conditions for the present problem can be described as follows:

Along the axis of the arterial segment $r = 0$, the radial velocity, axial velocity gradient, temperature gradient and spin of microrotation vanish,

$$i.e., \quad at \quad r = 0, \quad v = w = \frac{\partial u}{\partial r} = \frac{\partial \theta}{\partial r} = 0. \tag{19}$$

and at the arterial wall

$$i.e., \quad at \quad r = R(z,t), \quad u = w = 0, \quad \theta = 1 \quad and \quad v = \frac{\partial R}{\partial t}. \tag{20}$$

3. Transformation of the governing equations

For finding the numerical solution of the above system of equations using finite difference scheme, it is necessary to first transform the complex physical domain to a computational rectangular domain by introducing a radial coordinate transformation, given by

$$\xi = \frac{r}{R(z,t)}.$$

Using this transformation, Eqs. (15)–(18) are transformed to the equations

$$\frac{\partial u}{\partial z} - \frac{\xi}{R}\frac{\partial u}{\partial \xi}\frac{\partial R}{\partial z} + \frac{v}{\xi R} + \frac{1}{R}\frac{\partial v}{\partial \xi} = 0, \tag{21}$$

$$\frac{\partial u}{\partial t} = \frac{\frac{\partial u}{\partial \xi}}{R}\left[\xi\left(\frac{\partial R}{\partial t} + u\frac{\partial R}{\partial z}\right) - v\right] - u\frac{\partial u}{\partial z} + \frac{(1+K)}{\alpha^2 R^2}\left[\frac{\partial^2 u}{\partial \xi^2} + \frac{1}{\xi}\frac{\partial u}{\partial \xi}\right] + \frac{K}{\alpha^2 R}\left(\frac{\partial w}{\partial \xi} + \frac{w}{\xi}\right) + \frac{1}{\alpha^2}\left[G(t) - Ha^2 u - \frac{\partial p}{\partial z} - \frac{1}{K_p}u\right], \tag{22}$$

$$\frac{\partial w}{\partial t} = \frac{\frac{\partial w}{\partial \xi}}{R}\left[\xi\left(\frac{\partial R}{\partial t} + u\frac{\partial R}{\partial z}\right) - v\right] - u\frac{\partial w}{\partial z} - \frac{K}{\alpha^2 J}\left(2w - \frac{\partial v}{\partial z}\right) - \frac{K}{\alpha^2 J R}\left[\frac{\partial u}{\partial \xi} + \xi\frac{\partial v}{\partial \xi}\frac{\partial R}{\partial z}\right] + \frac{m}{\alpha^2 J R^2}\left[\frac{\partial^2 w}{\partial \xi^2} + \frac{1}{\xi}\frac{\partial w}{\partial \xi} - \frac{w}{\xi^2}\right], \tag{23}$$

$$\frac{\partial \theta}{\partial t} = \frac{\frac{\partial \theta}{\partial \xi}}{R}\left[\xi\left(\frac{\partial R}{\partial t} + u\frac{\partial R}{\partial z}\right) - v\right] - u\frac{\partial \theta}{\partial z} + \frac{1}{\alpha^2 P_r R^2}\left[\frac{\partial^2 \theta}{\partial \xi^2} + \frac{1}{\xi}\frac{\partial \theta}{\partial \xi}\right] + \frac{Br\,Ha^2}{\alpha^2 P_r}u^2 + \frac{(1+K)Br}{\alpha^2 P_r}\left[2\left(\frac{\partial u}{\partial z} - \frac{\xi}{R}\frac{\partial u}{\partial \xi}\frac{\partial R}{\partial z}\right)^2 + \frac{1}{R^2}\left(\frac{\partial u}{\partial \xi}\right)^2\right]. \tag{24}$$

Also, the boundary conditions (19) and (20) assume the form

$$v = w = \frac{\partial u}{\partial \xi} = \frac{\partial \theta}{\partial \xi} = 0 \quad at \quad \xi = 0. \tag{25}$$

and

$$u = w = 0, \quad v = \frac{\partial R}{\partial t} \quad and \quad \theta = 1 \quad at \quad \xi = 1. \tag{26}$$

Multiplying Eq. (21) by ξR and integrating with respect to ξ from 0 and ξ, we get

$$v(\xi, z, t) = \xi u\frac{\partial R}{\partial z} - \frac{R}{\xi}\int_0^{\xi} \xi\frac{\partial u}{\partial z}d\xi - \frac{2}{\xi}\frac{\partial R}{\partial z}\int_0^{\xi} \xi u d\xi. \tag{27}$$

Using the boundary condition (26) at $\xi = 1$, Eq. (27) becomes

$$\frac{1}{R}\frac{\partial R}{\partial t} = -\frac{2}{R}\frac{\partial R}{\partial z}\int_0^1 \xi u d\xi - \int_0^1 \xi\frac{\partial u}{\partial z}d\xi,$$

which can be rewritten in the form

$$\int_0^1 \xi\frac{\partial u}{\partial z}d\xi = \int_0^1 \xi\left[\frac{1}{R}\frac{\partial R}{\partial t}f(\xi) - \frac{2}{R}\frac{\partial R}{\partial z}u\right]d\xi. \tag{28}$$

Let us choose $f(\xi) = -4(\xi^2 - 1)$, so that $\int_0^1 \xi f(\xi)d\xi = 1$.

From (28), we have

$$\frac{\partial u}{\partial z} = \frac{4(\xi^2 - 1)}{R}\frac{\partial R}{\partial t} - \frac{2}{R}\frac{\partial R}{\partial z}u, \tag{29}$$

Substituting (29) into (27), we obtain the radial velocity in the following form

$$v(\xi, z, t) = \xi\left[u\frac{\partial R}{\partial z} + (2 - \xi^2)\frac{\partial R}{\partial t}\right]. \tag{30}$$

In the next section, we present a computational scheme, by using which, we can obtain the numerical solution for the axial velocity, microrotation components and the temperature variable governed by the Eqs. (22)–(24).

4. Computational scheme

For numerical computation, we subdivide the rectangular computational domain into a network by drawing straight lines parallel to the coordinate axes. Using the finite difference discretization technique together with Crank–Nicolson scheme, the transformed governing equations (22), (23), (24) and (30) are reduced to a system of linear algebraic equations. The solutions for $u(z, \xi, t)$, $v(z, \xi, t)$, $\theta(z, \xi, t)$ at any mesh point (i, j) in the computational domain may be denoted by $u^n_{i,j}$, $v^n_{i,j}$, $\theta^n_{i,j}$ respectively, in which $z_i = i * \triangle z, \quad i = 0, 1, 2, \ldots, M$;

Please cite this article as: G.C. Shit, S. Maiti, M. Roy et al., Pulsatile flow and heat transfer of blood in an overlapping vibrating atherosclerotic artery: A numerical study, Mathematics and Computers in Simulation (2019), https://doi.org/10.1016/j.matcom.2019.06.015.

$\xi_j = j * \triangle\xi, \quad j = 0, 1, 2, \ldots, N; \quad t_n = n * \triangle t, \quad n = 0, 1, 2, \ldots;$ where M and N are the maximum number of mesh points in the z and ξ directions respectively and n denotes the time step index.

Using FTCS scheme, the discretized equation (22) constitutes a tridiagonal system of the form

$$A^n_{i,j}u^{n+1}_{i,j-1} + B^n_{i,j}u^{n+1}_{i,j} + C^n_{i,j}u^{n+1}_{i,j+1} = D^n_{i,j}, \tag{31}$$

where

$$A^n_{i,j} = \frac{\triangle t}{4R^n_i\triangle\xi}\left[\xi_j\left(\left(\frac{\partial R}{\partial t}\right)^n_i + u^n_{i,j}\left(\frac{\partial R}{\partial z}\right)^n_i\right) - v^n_{i,j}\right] - \frac{(1+K)\triangle t}{\alpha^2(R^n_i)^2}\left(\frac{1}{2\triangle\xi^2} - \frac{1}{4\xi_j\triangle\xi}\right),$$

$$B^n_{i,j} = 1 + \frac{(1+K)\triangle t}{\alpha^2(R^n_i)^2\triangle\xi^2} + \frac{\triangle t}{\alpha^2}(Ha^2 + \frac{1}{K_p}) + \triangle t\left(\frac{u^n_{i+1,j} - u^n_{i-1,j}}{2\triangle z}\right),$$

$$C^n_{i,j} = -\frac{\triangle t}{4R^n_i\triangle\xi}\left[\xi_j\left(\left(\frac{\partial R}{\partial t}\right)^n_i + u^n_{i,j}\left(\frac{\partial R}{\partial z}\right)^n_i\right) - v^n_{i,j}\right] - \frac{(1+K)\triangle t}{\alpha^2(R^n_i)^2}\left(\frac{1}{2\triangle\xi^2} + \frac{1}{4\xi_j\triangle\xi}\right),$$

$$\begin{aligned} D^n_{i,j} &= u^n_{i,j} + \frac{\triangle t}{4R^n_i\triangle\xi}\left[\xi_j\left(\left(\frac{\partial R}{\partial t}\right)^n_i + u^n_{i,j}\left(\frac{\partial R}{\partial z}\right)^n_i\right) - v^n_{i,j}\right]\left(u^n_{i,j+1} - u^n_{i,j-1}\right) \\ &\quad + \frac{(1+K)\triangle t}{2\alpha^2(R^n_i)^2}\left[\frac{u^n_{i,j+1} - 2u^n_{i,j} + u^n_{i,j-1}}{\triangle\xi^2} + \frac{u^n_{i,j+1} - u^n_{i,j-1}}{2\xi_j\triangle\xi}\right] + \frac{\triangle t}{\alpha^2}(G(t) \\ &\quad - \frac{\partial p}{\partial z}) - \frac{\triangle t u^n_{i,j}}{2\triangle z}\left(u^n_{i+1,j} - u^n_{i-1,j}\right) + \frac{K\triangle t}{\alpha^2(R^n_i)^2}\left(\frac{w^n_{i,j+1} - w^n_{i,j-1}}{2\triangle\xi} + \frac{w^n_{i,j}}{\xi_j}\right). \end{aligned}$$

Similarly, the tridiagonal system corresponding to Eq. (23) is given by

$$P^n_{i,j}w^{n+1}_{i,j-1} + Q^n_{i,j}w^{n+1}_{i,j} + E^n_{i,j}w^{n+1}_{i,j+1} = S^n_{i,j}, \tag{32}$$

where

$$P^n_{i,j} = \frac{\triangle t}{4R^n_i\triangle\xi}\left[\xi_j\left(\left(\frac{\partial R}{\partial t}\right)^n_i + u^n_{i,j}\left(\frac{\partial R}{\partial z}\right)^n_i\right) - v^n_{i,j}\right] - \frac{M\triangle t}{\alpha^2 J(R^n_i)^2}\left(\frac{1}{2\triangle\xi^2} - \frac{1}{4\xi_j\triangle\xi}\right),$$

$$Q^n_{i,j} = 1 + \frac{M\triangle t}{\alpha^2 J(R^n_i)^2}\left(\frac{1}{\triangle\xi^2} + \frac{1}{\xi_j^2}\right) + \frac{2K\triangle t}{\alpha^2 J},$$

$$E^n_{i,j} = -\frac{\triangle t}{4R^n_i\triangle\xi}\left[\xi_j\left(\left(\frac{\partial R}{\partial t}\right)^n_i + u^n_{i,j}\left(\frac{\partial R}{\partial z}\right)^n_i\right) - v^n_{i,j}\right] - \frac{M\triangle t}{\alpha^2 J(R^n_i)^2}\left(\frac{1}{2\triangle\xi^2} + \frac{1}{4\xi_j\triangle\xi}\right),$$

$$\begin{aligned} S^n_{i,j} &= w^n_{i,j} + \frac{\triangle t}{4R^n_i\triangle\xi}\left[\xi_j\left(\frac{\partial R}{\partial t}\right)^n_i + u^n_{i,j}\left(\frac{\partial R}{\partial z}\right) - v^n_{i,j}\right]\left(w^n_{i,j+1} - w^n_{i,j-1}\right) \\ &\quad + \frac{M\triangle t}{2\alpha^2 J(R^n_i)^2}\left[\frac{w^n_{i,j+1} - 2w^n_{i,j} + w^2_{i,j-1}}{\triangle\xi^2} + \frac{w^n_{i,j+1} - w^n_{i,j-1}}{2\xi_j\triangle\xi}\right] \\ &\quad + \frac{K\triangle t}{\alpha^2 J}\left(\frac{v^n_{i+1,j} - v^n_{i-1,j}}{2\triangle z} - \frac{\xi_j}{R^n_i}\left(\frac{\partial R}{\partial t}\right)^n_i\frac{v^n_{i,j+1} - v^n_{i,j-1}}{2\triangle\xi}\right) \\ &\quad - \frac{K\triangle t}{\alpha^2 J R^n_i}\left(\frac{u^n_{i,j+1} - u^n_{i,j-1}}{2\triangle\xi}\right), \end{aligned}$$

and the tridiagonal system corresponding to Eq. (24) is given by

$$X^n_{i,j}\theta^{n+1}_{i,j-1} + Y^n_{i,j}\theta^{n+1}_{i,j} + Z^n_{i,j}\theta^{n+1}_{i,j+1} = W^n_{i,j}, \tag{33}$$

where

$$X^n_{i,j} = \frac{\triangle t}{4R^n_i\triangle\xi}\left[\xi_j\left(\left(\frac{\partial R}{\partial t}\right)^n_i + u^n_{i,j}\left(\frac{\partial R}{\partial z}\right)^n_i\right) - v^n_{i,j}\right] - \frac{\triangle t}{\alpha^2(R^n_i)^2 Pr}\left(\frac{1}{2\triangle\xi^2} - \frac{1}{4\xi_j\triangle\xi}\right),$$

$$Y^n_{i,j} = 1 + \frac{\triangle t}{\alpha^2 Pr(R^n_i)^2\triangle\xi^2},$$

Please cite this article as: G.C. Shit, S. Maiti, M. Roy et al., Pulsatile flow and heat transfer of blood in an overlapping vibrating atherosclerotic artery: A numerical study, Mathematics and Computers in Simulation (2019), https://doi.org/10.1016/j.matcom.2019.06.015.

$$Z^n_{i,j} = -\frac{\triangle t}{4R^n_i \triangle \xi}\left[\xi_j\left(\left(\frac{\partial R}{\partial t}\right)^n_i + u^n_{i,j}\left(\frac{\partial R}{\partial z}\right)^n_i\right) - v^n_{i,j}\right] - \frac{\triangle t}{\alpha^2 (R^n_i)^2 Pr}\left(\frac{1}{2\triangle \xi^2} + \frac{1}{4\xi_j \triangle \xi}\right),$$

$$\begin{aligned} W^n_{i,j} = {} & \theta^n_{i,j} + \frac{\triangle t}{4R^n_i \triangle \xi}\left[\xi_j\left(\left(\frac{\partial R}{\partial t}\right)^n_i + u^n_{i,j}\left(\frac{\partial R}{\partial z}\right)^n_i\right) - v^n_{i,j}\right]\left(\theta^n_{i,j+1} - \theta^n_{i,j-1}\right) \\ & + \frac{\triangle t}{2\alpha^2 Pr (R^n_i)^2}\left[\frac{\theta^n_{i,j+1} - 2\theta^n_{i,j} + \theta^n_{i,j-1}}{\triangle \xi^n} + \frac{\theta^n_{i,j+1} - \theta^n_{i,j-1}}{2\xi_j \triangle \xi}\right] \\ & + \frac{\triangle t Br Ha^2}{\alpha^2 Pr}(u^n_{i,j})^2 - \frac{\triangle t u^n_{i,j}}{2\triangle z}\left(\theta^n_{i+1,j} - \theta^n_{i-1,j}\right) \\ & + \frac{\triangle t(1+K)Br}{\alpha^2 Pr}\left[2\left(\frac{u^n_{i+1,j} - u^n_{i-1,j}}{2\triangle z} - \frac{\xi_j}{R^n_i}\left(\frac{\delta R}{\delta z}\right)^n_i (i)\frac{u^n_{i,j+1} - u^n_{i,j-1}}{2\triangle \xi}\right)^2\right. \\ & \left. + \frac{1}{(R^n_i)^2}\left(\frac{u^n_{i,j+1} - u^n_{i,j-1}}{2\triangle z}\right)^2\right]. \end{aligned}$$

The expression for radial velocity component in the discretized form may now be obtained from Eq. (30) as

$$v^n_{i,j} = \xi_j\left[u^n_{i,j}\left(\frac{\partial R}{\partial z}\right)^n_i + (2-\xi^2_j)\left(\frac{\partial R}{\partial t}\right)^n_i\right]. \tag{34}$$

After obtaining the solution for the radial component of velocity explicitly from (34) and substituting it into the Eqs. (31)–(33), we obtain the solutions for axial velocity, microrotation component and temperature. Once we have the solutions for u, v and θ, we can obtain the fluid acceleration F, the volumetric flow rate Q, wall shear stress (WSS) τ_w and the Nusselt number Nu by using the following relations:

$$F^{n+1}_{i,j} = \frac{u^n_{i,j+1} - u^n_{i,j-1}}{2\Delta\xi R^n_i}\left(\xi_j\left(\left(\frac{\partial R}{\partial t}\right)^n_i + u^n_{i,j}\left(\frac{\partial R}{\partial z}\right)^n_i\right) - v^n_{i,j}\right) - u^n_{i,j}\frac{u^n_{i+1,j} - u^n_{i-1,j}}{2\Delta z},$$

$$Q_i = 2\pi (R^n_i)^2 \int_0^1 \xi_j u^n_{i,j} d\xi_j,$$

$$\tau_w = \frac{(1+K)}{\alpha^2 (R^n_i)^2}\left(\frac{u^n_{i,N} - u^n_{i,N-1}}{2\Delta\xi}\right) + \frac{K}{\alpha^2 R^n_i} w^n_{i,N},$$

and

$$Nu_i = \frac{1}{R^n_i}\frac{\theta^n_{i,N} - \theta^n_{i,N-1}}{\Delta\xi}.$$

5. Results and discussion

Of concern in this investigation are in this the flow characteristics of blood, when it passes through a porous overlapping stenosed artery under the action of a periodic body acceleration and an externally applied magnetic field. In such an environment, with an aim to examine the flow behaviour of blood, we have taken up a specific numerical study for different flow characteristics of blood, by considering physiological data from the existing scientific literatures [15–17,23,27,45,51]. The computational work for the present study has been carried out by using the following values of physical parameters:

$$\frac{L}{R_0} = 10.0,\ d = 2.0,\ l_0 = 1.0, a_0 = 0.0, 1.0, 2.0, 3.0;\ b = 1.0,\ \phi_g = 0.0,$$
$$\phi_r = 0.0,\ R_0 = 1.0,\ \bar{R} = 1.0,\ A_p = 1.46,\ \bar{K} = 7.30,\ K_r = 0.05,\ f_p = 1.2,$$
$$K = 0.0, 0.1, 0.2, 0.3;\ J = 0.1,\ K_p = 0.1, 0.02, 0.03, 0.04, 0.05, 0.06, 1.0;$$
$$m = 0.1, 0.01, 0.001;\ \alpha = 3.0,\ Ha = 0, 1, 2, 3, 4;$$

and corresponding to human body temperature, $T = 310$K, the $P_r = 21$ has been taken for human blood. In order to examine the specific influence of the Prandtl number on the flow of blood, the computation has also been for $Pr = 14$ and 25. We have taken $\Delta\xi = 0.025$, $\Delta z = 0.05$, $\Delta t = 0.001$ through out the numerical computation. Also, we have considered $t = 7.414$, which is the time of systolic phase at a fully developed stage of blood flow.

Please cite this article as: G.C. Shit, S. Maiti, M. Roy et al., Pulsatile flow and heat transfer of blood in an overlapping vibrating atherosclerotic artery: A numerical study, Mathematics and Computers in Simulation (2019), https://doi.org/10.1016/j.matcom.2019.06.015.

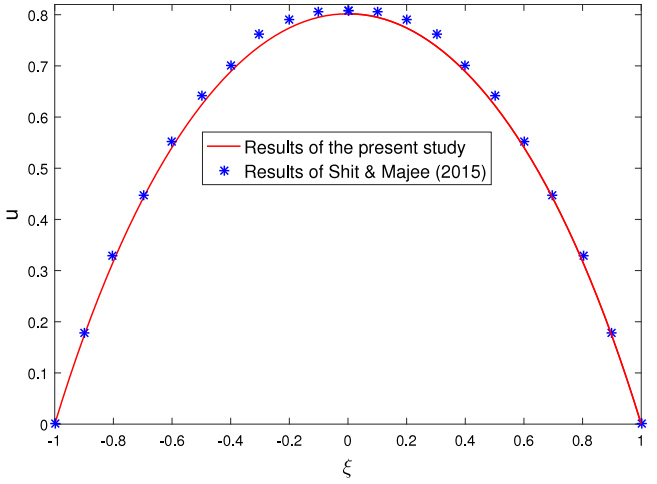

Fig. 2. Comparison of velocity profile u at the throat of the stenosis when we set $K = 0$, $m = 0$, $K_p = 1000$, $\alpha = 4$, $Ha = 2$, $Pr = 25$, $t = 7$, $\phi_g = \frac{\pi}{4}$, $\phi_r = 0$, $d = 3$, $l_0 = 1.85$.

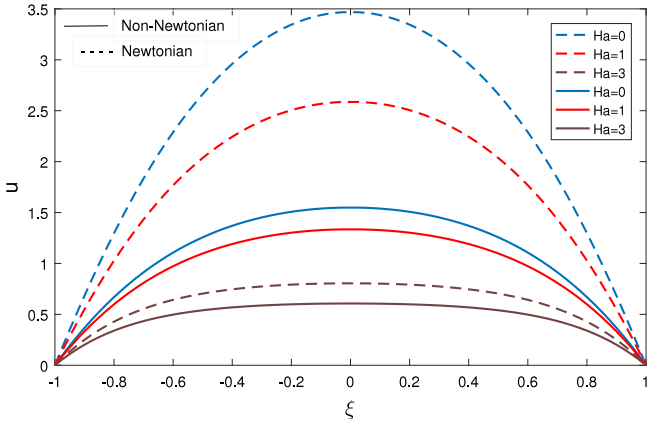

Fig. 3. Velocity distribution u at the throat of the stenosis for different values of the Hartmann number Ha, when $K = 0.1$, $K_p = 0.05$, $Pr = 21$, $t = 7.414$, $a_0 = 1.0$;.

We have noted that further reduction in the values of $\Delta\xi$ and Δz does not bring about any significant change. This observation ensures the stability of the numerical schemes used in this investigation.

The results for the velocity distribution, based on the present study have been validated through Fig. 2 that provides a comparison between the results of the present study with those of an earlier study [38] conducted by Shit and Majee in 2015. This figure clearly shows a very good agreement of the results of the two investigations, when $K = 0$, $m = 0$, $K_p = 1000$, $\alpha = 4$, $Ha = 2$, $Pr = 25$, $t = 7$, $\phi_g = \frac{\pi}{4}$, $\phi_r = 0$, $d = 3$, $l_0 = 1.85$. By employing the same code, other physical variables involved in the present study have been computed and their variations have been presented by means of graphs.

Figs. 3–5 illustrate the variation of blood velocity u along the radial direction of the stenosed artery for different values of the Hartmann number Ha, viscosity parameter K and the porous permeability parameter K_p respectively. In Fig. 3 dotted lines indicate the velocity distribution for a Newtonian fluid (corresponding to $K = 0$, $m = 0$) and solid lines represent that of the micropolar fluid. It shows that the velocity of blood, if considered as a Newtonian fluid is more than that when it is considered as a micropolar fluid. The additional viscosity generated due to the microrotation of microparticles suspended in the blood stream may be considered to be responsible for the reduction in the case of a micropolar fluid model, which is assumed to represent blood in the present study. From the same figure one may further observe that the velocity diminishes with the increase of the Hartmann number Ha. The

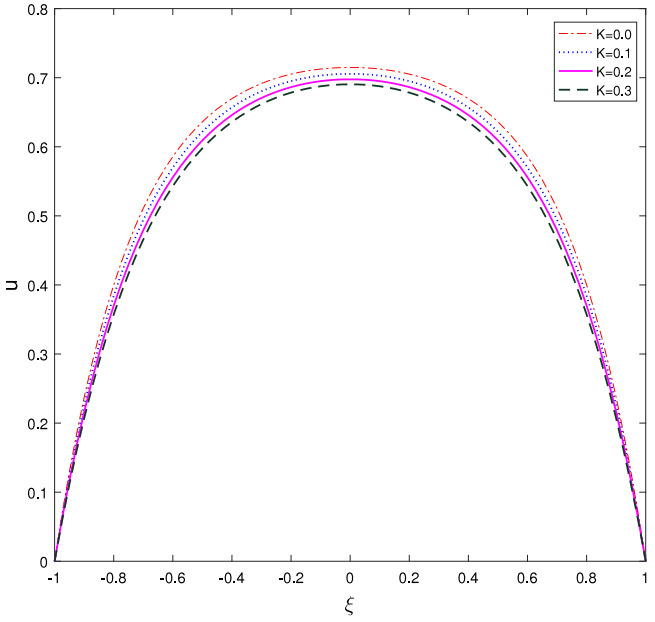

Fig. 4. Velocity distribution u at the throat of the stenosis for different values of K, when $Ha = 1.0$, $K_p = 0.05$, $Pr = 21$, $t = 7.414$, $a_0 = 1.0$;.

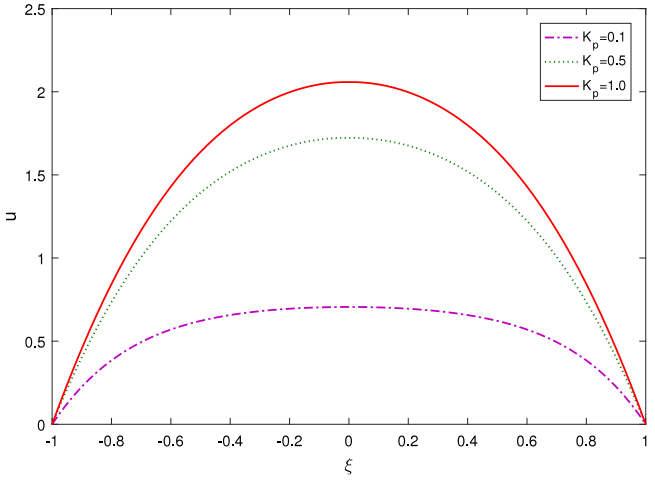

Fig. 5. Velocity distribution u at the throat of the stenosis for different values of K_p, when $Ha = 1.0$, $K = 0.1$, $Pr = 21$, $t = 7.414$, $a_0 = 1.0$.

reason is that due to the application of the magnetic field, Lorentz force is developed, that opposes the fluid motion. The velocity attains its maximum at the axis of the artery in all the three cases examined here (see Fig. 3). From Fig. 3, one may further note that under the influence of a sufficiently strong magnetic field, the motion of blood in the artery may stop altogether. Fig. 4 depicts the velocity variation for different values of the viscosity ratio $K = \frac{k}{\mu}$. We find that as K increases, blood velocity diminishes. Fig. 5 shows that the velocity increases with a rise in the porous permeability parameter K_p. Physically, as the porous permeability increases, the frictional force reduces, and so the fluid velocity is likely to increase. The increase in microrotation of blood cells in the lumen of the artery can be responsible for such an observation.

Please cite this article as: G.C. Shit, S. Maiti, M. Roy et al., Pulsatile flow and heat transfer of blood in an overlapping vibrating atherosclerotic artery: A numerical study, Mathematics and Computers in Simulation (2019), https://doi.org/10.1016/j.matcom.2019.06.015.

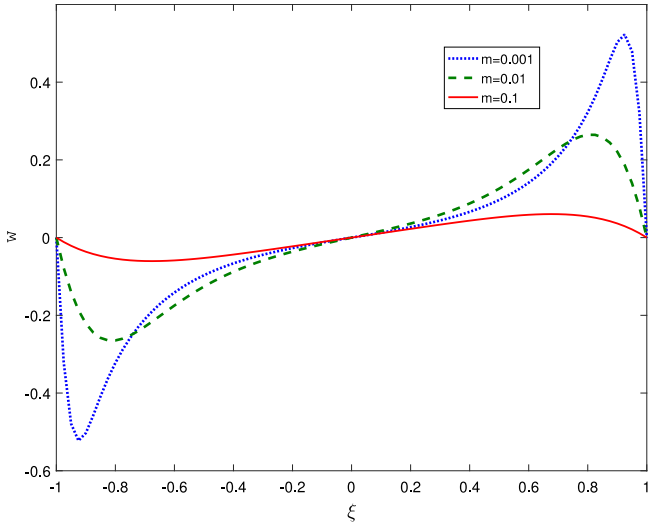

Fig. 6. Variation of microrotation component w at the throat of the stenosis for different values of m, when $K = 0.1$, $J = 0.1$, $Ha = 1$;.

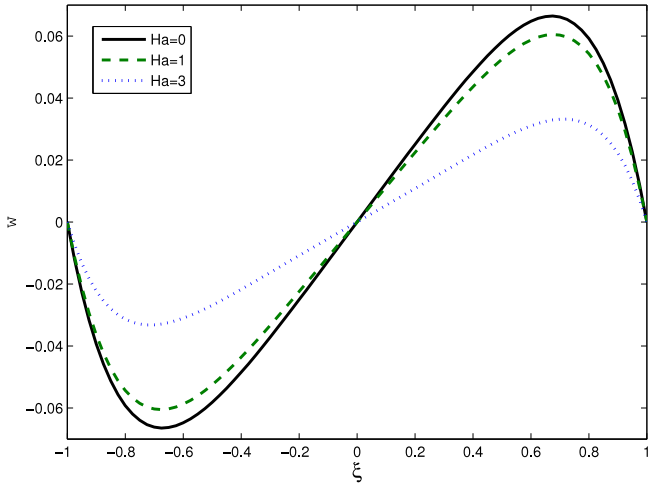

Fig. 7. Variation of microrotation component w at the throat of the stenosis for different values of Ha, when $m = 0.1$, $J = 0.1$, $Ha = 1$;.

Figs. 6–8 depict the variation of microrotation component w along the radial direction of the artery for different values of the micropolar parameter m, Hartmann number Ha and permeability of the porous medium. Fig. 6 shows that the microrotation component decreases in the lower portion of the stenosed artery with an increase in the micropolar parameter m. However, at the axis of the artery, the microrotational component is independent of m. The opposite trend is observed on the other side of the stenosed artery. This happens, because reduction in m causes elevation in the viscosity coefficient μ and thereby microrotation velocity is reduced. Fig. 7 shows that the microrotation velocity increases in magnitude with a rise in the magnetic field strength. However, the trend is reversed in the case of porous permeability parameter K_p as shown in Fig. 8. In these figures, it is interesting to observe that the rotational velocity w creates two lobes on either side of the axis of the artery. The lobes rotate in different directions. The positive component of w acts in the direction of blood flow. The centre of these lobes shifts towards the central axis of the artery for increasing values of m, Ha and K_p.

Figs. 9–11 describe the change in the volumetric flow rate Q, when there is a change in the parametric values. Fig. 9 gives the time-variations of the volumetric flow rate Q for different strengths of the applied magnetic field. It is seen that the flow rate Q is periodic in time t and the amplitude of periodic flow rate diminishes, as the

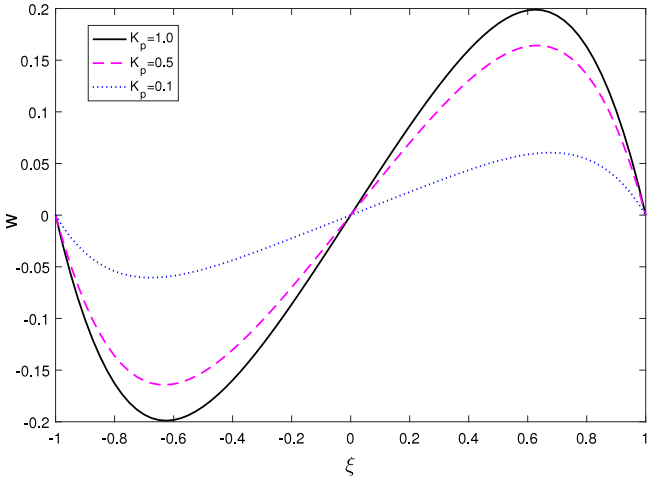

Fig. 8. Variation of microrotation component w at the throat of the stenosis for different values of K_p, when $m = 0.1$, $J = 0.1$, $Ha = 1$.

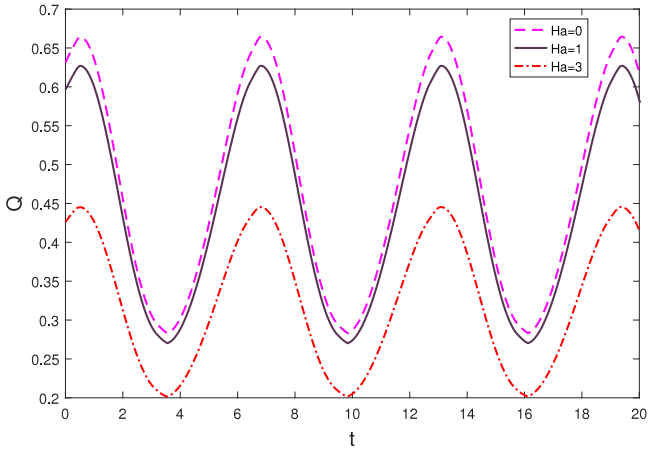

Fig. 9. Time-variation of the volumetric flow rate Q, for different values of Ha, when $K = 0.1$, $K_p = 0.05$, $a_0 = 1.0$.

magnetic field strength increases. It has the same behaviour as that of the velocity profile, since the flow rate is directly proportional to the axial velocity u. Fig. 10 represents the volumetric flow rate variation with time t for different values of the viscosity parameter K. It is observed that the flow rate Q reduces, as the viscosity parameter K increases. It may be interpreted by saying that as K increases, the viscosity due to rotation of microparticles suspended in blood increases and thereby flow rate is reduced. The change in volumetric flow rate along the length of the arterial segment having overlapping stenosis has been presented in Fig. 11 for different amplitudes of the body acceleration. We observe from this figure that the volumetric flow rate Q increases gradually with an enhancement of the amplitude of body acceleration. This implies that in the vibration environment, the blood flow velocity increases, but the enhancement of blood flow can be controlled by applying a magnetic field of suitable strength. It thus turns out that these two external body forces are crucial for controlling blood flow rate.

Figs. 12–14 depict the nature of distribution of the fluid acceleration F for different values of the amplitude of body acceleration, Hartmann number Ha and porous permeability parameter K_p. In each of these cases, the fluid acceleration F is maximum at the axis of the artery and then it gradually diminishes and ultimately vanishes at the wall of the artery, satisfying the no-slip condition at the wall. It is observed from Fig. 12 that the magnitude of fluid acceleration F increases as the amplitude of body acceleration increases. Thus fluid acceleration is enhanced due to the vibration environment. However, from Fig. 13, we find that the magnitude of the fluid acceleration F decreases with the increase in Hartmann number Ha. This implies that the fluid acceleration F can be controlled

Please cite this article as: G.C. Shit, S. Maiti, M. Roy et al., Pulsatile flow and heat transfer of blood in an overlapping vibrating atherosclerotic artery: A numerical study, Mathematics and Computers in Simulation (2019), https://doi.org/10.1016/j.matcom.2019.06.015.

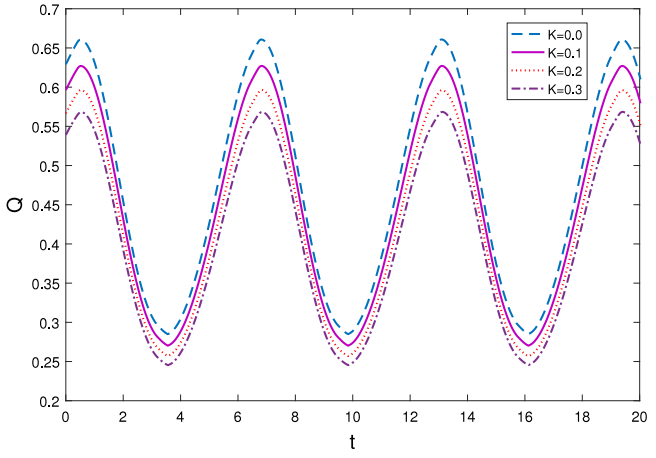

Fig. 10. Time-variation of the volumetric flow rate Q for different values of K, when $Ha = 1.0$, $K_p = 0.05$, $a_0 = 1.0$;.

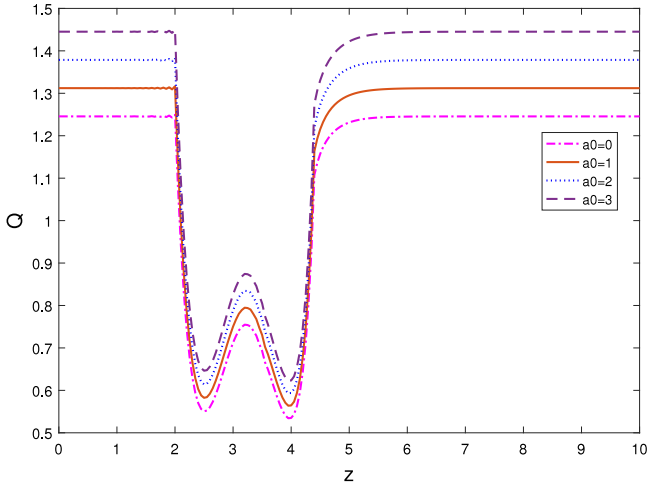

Fig. 11. Spatial-variation of the volumetric flow rate Q for different values of a_0, when $K = 0.1$, $K_p = 0.05$, $Ha = 1.0$;.

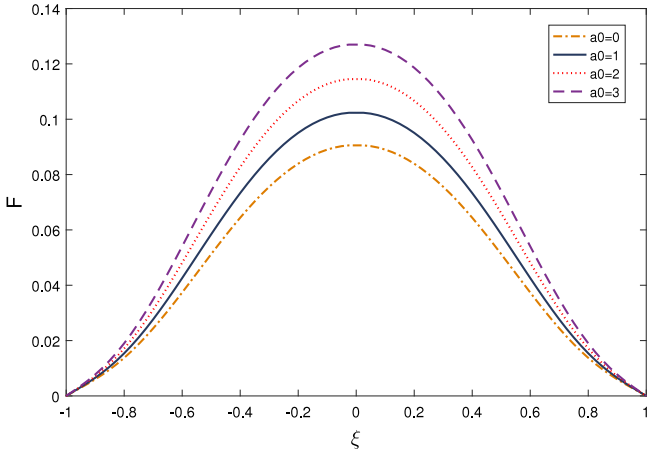

Fig. 12. Variation of fluid acceleration F along the radial direction for different amplitudes of the body acceleration a_0, when $Ha = 1.0$, $K_p = 0.05$.

Please cite this article as: G.C. Shit, S. Maiti, M. Roy et al., Pulsatile flow and heat transfer of blood in an overlapping vibrating atherosclerotic artery: A numerical study, Mathematics and Computers in Simulation (2019), https://doi.org/10.1016/j.matcom.2019.06.015.

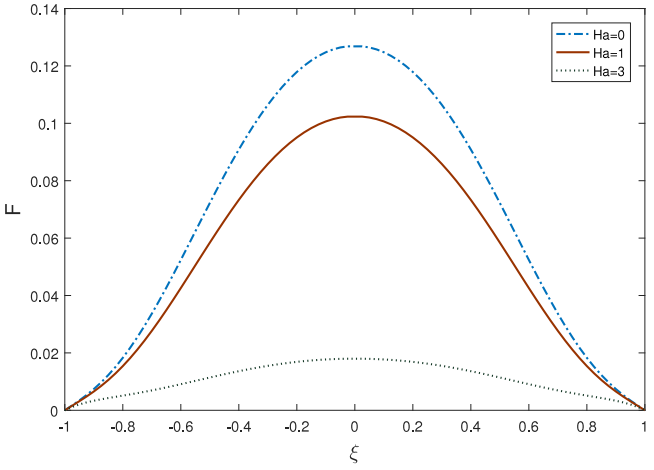

Fig. 13. Variation of fluid acceleration F along the radial direction for different values of Ha, when $a_0 = 1.0$, $K_p = 0.05$.

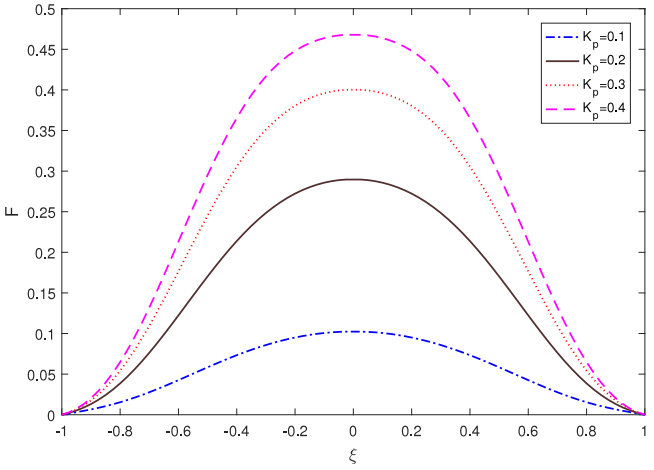

Fig. 14. Variation of fluid acceleration F along the radial direction for different values of K_p, when $a_0 = 1.0$, $Ha = 1.0$.

by suitably adjusting the intensity of the magnetic field. Fig. 14 shows that the fluid acceleration F increases with a rise in permeability. It is important to note that the porous permeability of flow passage has also controlling effect on blood flow.

Another important characteristic of blood flow is the wall shear stress τ_w. Its variation along the axial direction and with time are illustrated through Figs. 15–17. Fig. 15 shows that the wall shear stress increases as the permeability of the porous medium increases. It is observed that the wall shear stress (WSS) completely depends upon the geometry of the arterial wall. The wall shear stress is low at the secondary stenosis and therefore there is a possibility of further deposition of cholesterol at the downstream of the overlapping stenosis. This can be avoided by enhancing the permeability of the porous medium. Fig. 16 shows that with a rise in the Hartmann number Ha, the wall shear stress is reduced. Further formation of plaques in the endothelial layer of the artery can be possible. It is also noted that the wall shear stress changes periodically with time. However, Fig. 17 shows that the body acceleration can elevate the wall shear stress during systolic phase, while in the diastolic phase, the wall shear stress is reduced with an increase in body acceleration. Thus further deposition of cholesterol is more likely during diastole.

Figs. 18 and 19 illustrate the distribution of temperature θ at the middle of the stenosis for different values of Hartmann number Ha and Brinkman number Br. Figs. 18 and 19 indicate that the temperature θ increases as the Hartmann number Ha/ Brinkman number Br is increased. This observation can be useful for the hyperthermic

Please cite this article as: G.C. Shit, S. Maiti, M. Roy et al., Pulsatile flow and heat transfer of blood in an overlapping vibrating atherosclerotic artery: A numerical study, Mathematics and Computers in Simulation (2019), https://doi.org/10.1016/j.matcom.2019.06.015.

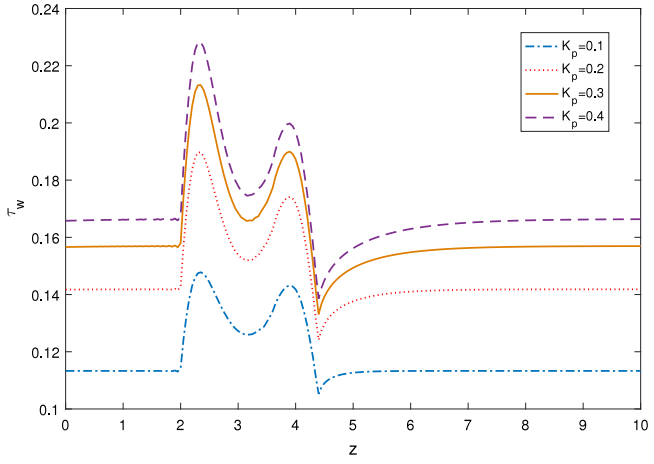

Fig. 15. Variation of wall shear stress τ_w along the axis of the artery for different values of K_p, when $a_0 = 1.0$, $Ha = 1.0$, $K = 0.1$.

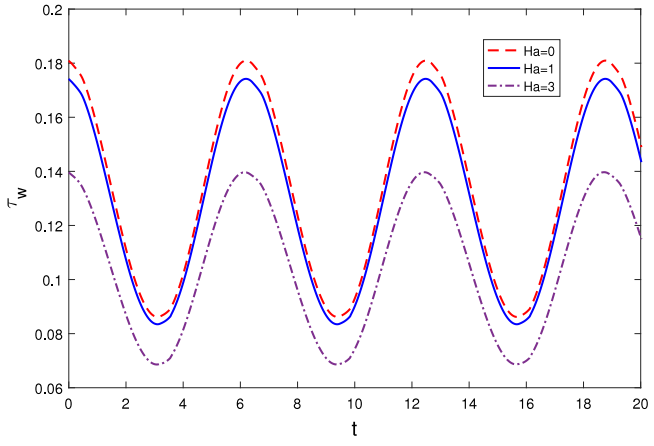

Fig. 16. Time variation of wall shear stress τ_w for different values of Ha, when $a_0 = 1.0$, $\alpha = 3.0$, $K = 0.1$;.

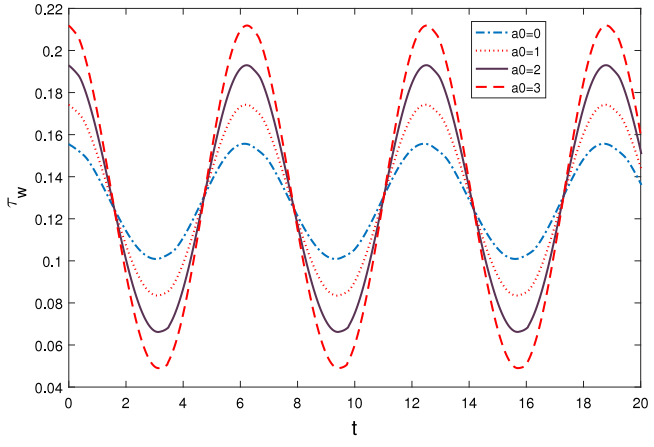

Fig. 17. Time variation of wall shear stress τ_w for different values of a_0, when $Ha = 1.0$, $\alpha = 3.0$, $K = 0.1$.

Please cite this article as: G.C. Shit, S. Maiti, M. Roy et al., Pulsatile flow and heat transfer of blood in an overlapping vibrating atherosclerotic artery: A numerical study, Mathematics and Computers in Simulation (2019), https://doi.org/10.1016/j.matcom.2019.06.015.

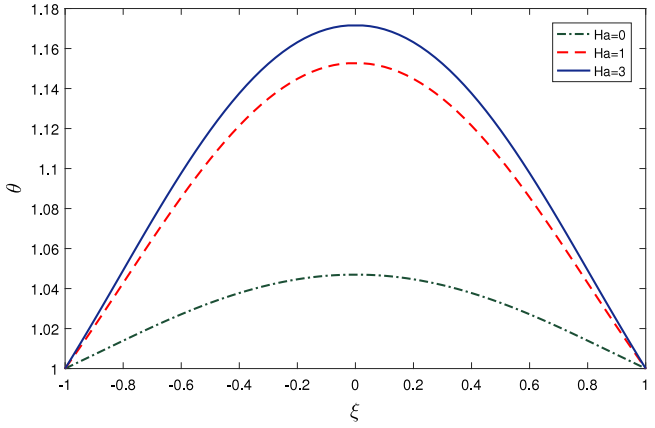

Fig. 18. Distribution of temperature θ for different values of Ha, when $a_0 = 1.0$, $b = 1.0$, $\phi_g = 0.0$, $\phi_r = 0.0$, $K = 0.1$, $Pr = 21$, $\alpha = 2.0$, $Br = 0.05$.

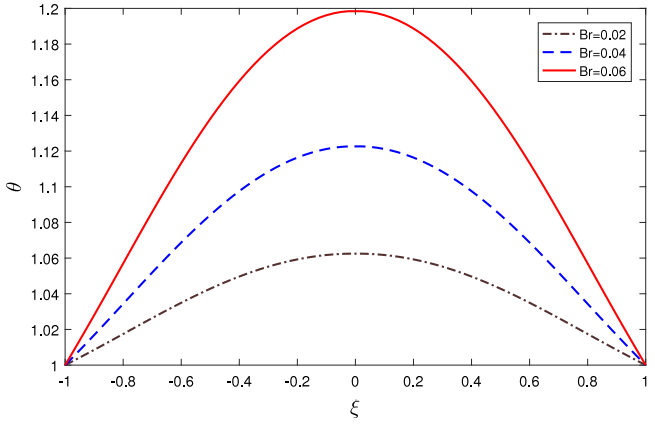

Fig. 19. Distribution of temperature θ for different values of Br, when $a_0 = 1.0$, $b = 1.0$, $\phi_g = 0.0$, $\phi_r = 0.0$, $K = 0.1$, $Pr = 21$, $\alpha = 2.0$, $Ha = 1.0$.

treatment of tumor/ cancer cells. The dissipation of energy due to fluid friction and the applied magnetic field can lead to an increase in temperature of blood. Thus, if studies are performed by ignoring the dissipation of energy, the temperature will be over-estimated.

Fig. 20 represents the variation of Nusselt number Nu (the rate of heat transfer at the arterial wall) along the axial direction z. We observe that Nusselt number is increased with a rise in the value of the Prandtl number Pr. It implies that the rate of heat transfer increases in the secondary stenosis region, while the heat transfer is comparatively low at the primary stenosis zone. The lowering of the Nusselt number is observed more at the down stream of the stenosis than in the upstream.

Fig. 21 gives the variation of Nusselt number Nu versus Hartmann number Ha for different values of the Brinkman number Br. Here one may make an observation that the Nusselt number increases with increasing values of the Brinkman number. It implies that owing to the dissipation of energy caused due to the viscosity of blood and the influence of the magnetic field, the heat transfer rate is enhanced. This effect is more pronounced, because of the extra viscosity due to the rotational effect of micro-elements. It is further observed from this figure that Nusselt number increases, when Hartmann number increases up to $Ha = 1.5$, beyond which it gets reduced gradually and then becomes constant for higher intensities of the externally applied magnetic field. This result will be of interest to the oncologists in the treatment of malignant tumor patients.

Please cite this article as: G.C. Shit, S. Maiti, M. Roy et al., Pulsatile flow and heat transfer of blood in an overlapping vibrating atherosclerotic artery: A numerical study, Mathematics and Computers in Simulation (2019), https://doi.org/10.1016/j.matcom.2019.06.015.

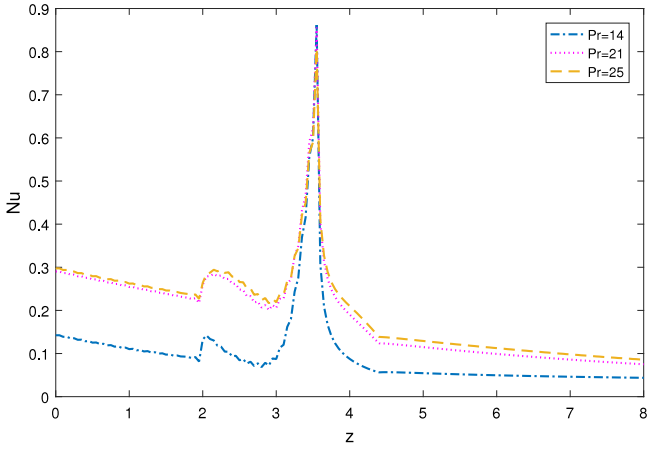

Fig. 20. Variation of Nusselt number Nu along the arterial axis for different values of Pr, when $K = 0.1$, $\alpha = 2.0$, $Ha = 1.0$.

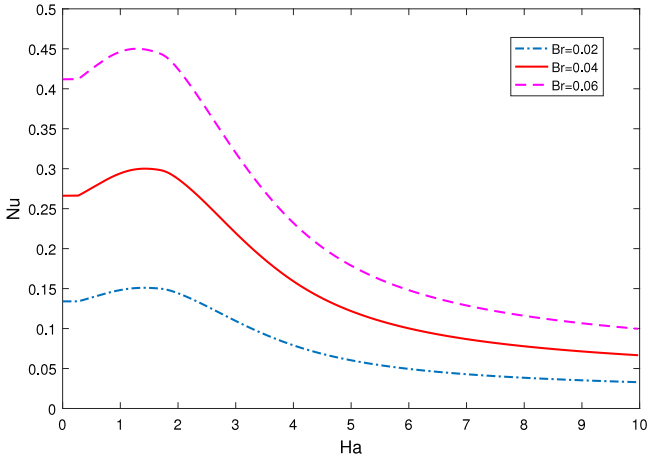

Fig. 21. Change in Nusselt number Nu for different values of Br, when $K = 0.1$, $Pr = 21$, $\alpha = 2.0$, $Ha = 1.0$.

6. Concluding remarks

This paper aims to investigate the pulsatile flow of blood through a porous overlapping stenosed artery in presence of an externally applied magnetic field under the influence of body acceleration. Micropolar fluid model is considered to represent non-Newtonian characteristics of blood, in order to investigate the microrotation effect of different microparticles suspended in blood. The problem is solved numerically by developing an implicit Crank–Nicolson finite difference scheme. The following conclusions can be drawn on the basis of the study.

- The rate of heat transfer increases during blood flow in the artery with an increase in the intensity of the externally applied magnetic field and also with an increase in Brinkman number.
- Wall shear stress changes periodically with time and gets reduced by increasing the magnetic field strength.
- Wall shear stress increases with a rise in the value of the permeability parameter.
- Fluid acceleration is enhanced when the permeability parameter/ amplitude of body acceleration is increased.
- Volumetric flow rate diminishes, when there is an increase in rotational viscosity.
- The downstream of the stenosis is greatly affected by most of the parameters involved in the study.

Finally, various recent works [18,37] on the effects of porosity in the flow of nanofluids are demonstrated clearly to motivate us for further work in the field of nano-biofluid.

Please cite this article as: G.C. Shit, S. Maiti, M. Roy et al., Pulsatile flow and heat transfer of blood in an overlapping vibrating atherosclerotic artery: A numerical study, Mathematics and Computers in Simulation (2019), https://doi.org/10.1016/j.matcom.2019.06.015.

Acknowledgements

The authors are grateful to the esteemed reviewers for their comments and suggestions to improve the quality of this article. The author, Prof J.C. Misra and the authors G.C. Shit and S. Maiti wish to thank the Science and Engineering Research Board (SERB), Department of Science and Technology, Govt. of India, New Delhi for the financial support through Grant Nos. CRG/2018/000153 and EEQ/2016/000050 respectively.

References

[1] M. Abdulhameed, M.M. Muhammad, A.Y. Gital, D.G. Yakubu, I. Khan, Effect of fractional derivatives on transient MHD flow and radiative heat transfer in a micro-parallel channel at high zeta potentials, Physica A 519 (2019) 42–71.
[2] I. Abdullah, N. Amin, A micropolar fluid model of blood flow through a tapered artery with a stenosis, Math. Methods Appl. Sci. 33 (2010) 1910–1923.
[3] R.R. Burton, S.D. Levert Jr., E.D. Mischaelsow, Man at high sustained $+G_z$ acceleration, A review, Aerosp. Med. 46 (1974) 1251–1253.
[4] C.G. Caro, T.J. Pedley, R.C. Schroter, W.A. Seed, The Mechanis of the Circulation, Oxford University Press, Oxford, 1978.
[5] S. Chandra, J.C. Misra, Influence of hall current and microrotation on the boundary flow of an electrically conducting fluid: Application to hemodynamics, J. Mol. Liq. 224 (Part A) (2016) 818–824.
[6] G.R. Charya, Flow of micropolar fluid through a constricted channel, Internat. J. Engrg. Sci. 15 (1977) 719–725.
[7] P. Chaturani, V. Palanisamy, Pulsatile flow of power law fluid model for blood flow under periodic body acceleration, Biorheology 27 (1990) 747–758.
[8] S. Chien, Hemorheology in clinical medicine, Recent Adv. Cardio Vascu. Dis. 2 (suppl.) (1981) 21.
[9] M.A. Elkot, W. Abbas, Numerical technique of blood flow through catheterized arteries with overlapping stenosis, Comput. Meth. Biomech. Biomed. Eng. 20 (1) (2017) 45–58.
[10] A.C. Erigen, Theory of micropolar fluids, J. Math. Mech. 16 (1966) 1–18.
[11] A.C. Eringen, Simple microfuids, Internat. J. Engrg. Sci. 2 (1964) 205–217.
[12] F. He, L. Hua, L. Gao, Effects of porosity in a seepage model on hemodynamics, J. Mech. Med. Biol. 17 (2017) 1740017.
[13] H.A. Hogan, M. Henriksen, An evaluation of a micropolar model for blood flow through an idealized stenosis, J. Biomech. 22 (3) (1989) 211–218.
[14] M.A. Imran, M. Aleem, M.B. Riaz, R. Ali, I. Khan, A comprehensive report on convective flow of fractional (ABC) and (CF) MHD viscous fluid subject to generalized boundary conditions, Chaos Solitons Fractals 118 (2019) 274–289.
[15] A.R. Khaled, K. Vafai, The role of porous media in modelling flow and heat transfer in biological tissues, Int. J. Heat Mass Transfer 46 (2003) 4989–5003.
[16] A.D. Kirwan Jr., Boundary conditions for micropolar fluids, Internat. J. Engrg. Sci. 24 (7) (1986) 1237–1242.
[17] J.S. Lee, Y.C. Fung, Flow in locally constricted tubes at low Reynolds numbers, J. Appl. Mech. 37 (1970) 9–16.
[18] Z. Li, I. Khan, A. Shafee, I. Tlili, T. Asifa, Energy transfer of Jeffery–Hamel nanofluid flow between non-parallel walls using Maxwell–Garnetts (MG) and Brinkman models, Energy Rep. 4 (2018) 393–399.
[19] D.W. Liepsch, Flow in tubes and arteries - A comparison, Biorheology 23 (4) (1986) 395–433.
[20] D.A. MacDonald, Blood Flow in Arteries, Edward Arnold, London, 1974.
[21] J.C. Misra, S.D. Adhikary, B. Mallick, A. Sinha, Mathematical modeling blood flow in arteries subject to a vibrating environment, J. Mech. Med. Biol. 18 (2018) 185001.
[22] J.C. Misra, S.D. Adhikary, G.C. Shit, Mathematical analysis of blood flow through an arterial segment with time dependent stenosis, Math. Model. Anal. 13 (2008) 401–412.
[23] J.C. Misra, S. Chakravarty, Flow in arteries in the presence of stenosis, J. Biomech. 19 (1986) 907–918.
[24] J.C. Misra, S. Chandra, H. Herwig, Flow of a micropolar fluid in a microchannel under the action of an alternating electric field: Estimates of blood flow bio-fluidic devices, J. Hydrodyn. 27 (2015) 350–358.
[25] J.C. Misra, S. Maiti, Peristaltic transport of rheological fluids: model for movement of food bolus through esophagus, Appl. Math. Mech. 33 (2012) 315–332.
[26] J.C. Misra, B. Pal, A mathematical model for the study of pulsatile flow of blood flow under an externally imposed body acceleratio, Math. Comput. Model. 29 (1999) 89–106.
[27] J.C. Misra, M.K. Patra, S.C. Misra, A non-Newtonian fluid model for blood flow through arteries under stenotic conditions, J. Biomech. 26 (1993) 1129–1141.
[28] J.C. Misra, B.K. Sahu, Flow through blood vessels under the action of a periodic acceleration field, Comput. Math. Appl. 16 (1988) 993–1016.
[29] J.C. Misra, G.C. Shit, Role of slip velocity in blood flow through stenosed arteries: A non-Newtonian model, J. Mech. Med. Biol. 7 (2007) 337–353.
[30] J.C. Misra, G.C. Shit, S. Chandra, P.K. Kundu, Electro-osmotic flow of a viscoelastic fluid in a channel: Applications to physiological fluid mechanics, Appl. Math. Comput. 2017 (2011) 7932–7939.
[31] J.C. Misra, G.C. Shit, R. Pramanik, Non-Newtonian flow of blood in a catheterized bifurcated stenosed artery, J. Bionic Eng. 15 (2018) 173–184.
[32] J.C. Misra, A. Sinha, G.C. Shit, Theoretical analysis of blood flow through an arterial segment having multiple stenosis, J. Mech. Med. Biol. 8 (2008) 265–279.

Please cite this article as: G.C. Shit, S. Maiti, M. Roy et al., Pulsatile flow and heat transfer of blood in an overlapping vibrating atherosclerotic artery: A numerical study, Mathematics and Computers in Simulation (2019), https://doi.org/10.1016/j.matcom.2019.06.015.

[33] J.C. Misra, A. Sinha, G.C. Shit, Mathematical modeling of blood flow in a porous vessel having double stenosis in the presence of an external magnetic field, Int. J. Biomath. 4 (2011) 207–225.
[34] P. Muthu, B.V.R. Kumar, P. Chandra, On the inference of wall properties in the peristaltic motion of micropolar fluid, ANZIAM J. 45 (2003) 245–260.
[35] R. Ponalagusamy, S. Priyadharshini, Couple stress fluid model for pulsatile flow of blood in a porous tapered arterial stenosis under magnetic field and periodic body acceleration, J. Mech. Med. Biol. 17 (2017) 1750109.
[36] N.D. Raihi, R. Roy, S. Cavazos, On arterial blood flow in the presence of an overlapping stenosis, Math. Comput Mod. 54 (2011) 2999–3006.
[37] M. Saqib, I. Khan, S. Shafie, Application of Atangana–Baleanu fractional derivative to MHD channel flow of CMC-based-CNTs nanofluid through a porous medium, Chaos Solitons Fractals 116 (2018) 79–85.
[38] G.C. Shit, S. Majee, Pulsatile flow of blood and heat transfer with variable viscosity under magnetic and vibration environment, J. Magn. Magn. Mater. 388 (2015) 106–115.
[39] G.C. Shit, S. Majee, Computational modeling of blood and heat transfer enhancement in a slowly varying arterial segment, Int. J. Heat Fluid Flow 70 (2017) 1750109.
[40] G.C. Shit, S. Majee, Magnetic field interaction with blood flow and heat transfer through diseased artery having Abdominal Aortic Aneurysm, Eur. J. Mech. B Fluids 71 (2018) 1–14.
[41] G.C. Shit, M. Roy, Pulsatile flow and heat transfer of a magneto-micropolar fluid through a stenosed artery under the influence of body acceleration, J. Mech. Med. Biol. 11 (2011) 643–661.
[42] G.C. Shit, M. Roy, Effect of slip velocity on peristaltic transport of a magneto-micropolar fluid through a porous non-uniform channel, Int. J. Appl. Comput. Math. 1 (2015) 121–141.
[43] A. Sinha, J.C. Misra, Numerical study of flow and heat transfer during oscillating blood flow in diseased arteries in presence of magnetic fields, Appl. Math. Mech. 33 (2012) 649–662.
[44] A. Sinha, J.C. Misra, MHD flow of blood through a dually stenosed artery: Effects of viscosity variation, variable hematocrit and velocity-slip, Canad. J. Chem. Eng. 92 (2014) 23–31.
[45] L.M. Srivastava, Flow of couple stress fluid through stenotic blood vessels, J. Biomech. 18 (1985) 479–485.
[46] V.K. Sud, G.S. Sekhon, Blood flow subject to a single cycle of body acceleration, Bull. Math. Biol. 46 (1984) 937–949.
[47] A. Tanveer, T. Hayat, A. Alsaedi, Peristaltic flow of MHD Jeffery nanofluid in curved channel with convective boundary conditions: a numerical study, Neural. Comput. Appl. 30 (2018) 437–446.
[48] A. Tanveer, T. Hayat, A. Alsaedi, B. Ahmad, On modified Darcys law utilization in peristalsis of Sisko fluid, J. Mol. Liq. 236 (2017) 290–297.
[49] A. Tanveer, T. Hayat, A. Alsaedi, B. Ahmad, Heat transfer analysis for peristalsis of MHD Carreau fluid in a curved channel through modified darcy law, J. Mech. (2018) http://dx.doi.org/10.1017/jmech.2018.38.
[50] R. Vanatham, S. Parvathamma, Flow of micropolar fluid through a tube with stenosis, Med. Bio. Eng. Comput. 21 (1983) 438–445.
[51] D.F. Young, Fluid mechanics of arterial stenosis, J. Biomech. Eng. 101 (1979) 157–175.

Please cite this article as: G.C. Shit, S. Maiti, M. Roy et al., Pulsatile flow and heat transfer of blood in an overlapping vibrating atherosclerotic artery: A numerical study, Mathematics and Computers in Simulation (2019), https://doi.org/10.1016/j.matcom.2019.06.015.